Ordered Mesoporous $BiVO_4$ through Nanocasting: A Superior Visible Light-Driven Photocatalyst

Guisheng Li, Dieqing Zhang, and Jimmy C. Yu*

Department of Chemistry, Environmental Science Program, and Center of Novel Functional Molecules, The Chinese University of Hong Kong, Shatin, New Territories, Hong Kong, China

Received January 24, 2008. Revised Manuscript Received March 26, 2008

This paper describes a nanocasting synthesis of ordered mesoporous bismuth vanadate ($BiVO_4$) crystals using bismuth nitrate hydrate and ammonia metavanadate as bismuth and vanadium sources and silica (KIT-6) as a template. Monoclinic scheelite $BiVO_4$ crystals were formed inside the mesopores of silica through a mild thermal process, and $BiVO_4$ was obtained after the removal of the hard template (silica) by NaOH treatment. As compared to conventional $BiVO_4$, the product exhibited a superior photocatalytic performance in the photochemical degradation of methylene blue and photocatalytic oxidation of NO gas in air under visible light irradiation. The product was characterized by using X-ray diffraction, the Brunauer−Emmett−Teller method, UV−vis light reflectance, X-ray photoelectron spectroscopy, Raman spectroscopy, and transmission electron microscopy. The relationship between the physicochemical property and the photocatalytic performance of the as-prepared samples is discussed.

Introduction

The depletion of energy resources and the degradation of the natural environment are two of the most urgent issues facing modern society. Visible light-driven photocatalytic technology can help to alleviate both problems by splitting water for green energy hydrogen production and degrading toxic pollutants.[1,2] At present, titanium dioxide (TiO_2) is the most widely used and most intensely studied photocatalyst, due to its low cost, nontoxicity, and high efficiency.[3,4] However, TiO_2 can only be activated with UV light, which accounts for only 4% of the solar energy that reaches the Earth's surface.[5] There is therefore an urgent need to develop photocatalysts that respond to visible light, and this important field of research has attracted considerable attention in recent years.

Bismuth vanadate ($BiVO_4$)-based compounds have been extensively investigated during the past two decades, and these lead-, cadmium-, and chromate-free inorganic yellow pigments have been used to manufacture brilliant yellow shades with a good gloss and hiding power.[6] With a short band gap of 2.4 eV, $BiVO_4$ is also an important visible light responsive photocatalyst and has been widely used in the evolution of photocatalytic O_2 and the photocatalytic degradation of organic pollutants.[7,8] Because of its excellent response to visible light, it has been widely studied as a potentially attractive advanced material for photocatalytic application. There are three naturally occurring crystal forms of $BiVO_4$, namely, tetragonal zircon, monoclinic scheelite, and tetragonal scheelite. Of these three crystal forms, monoclinic scheelite delivers the best photocatalytic performance under visible light irradiation and also has the strongest coloristic property.[9] Following the first reports of the experimental preparation of bismuth vanadate crystals,[13] various methods of synthesizing monoclinic scheelite $BiVO_4$ have been developed, including aqueous,[7] solid-state,[10] and hydrothermal processes[11] and organometallic decomposition.[12] However, to the best of our knowledge, all of the $BiVO_4$ samples produced in this way are nonporous and also have a very low surface area and a large crystal size. It has been demonstrated that a large surface area is a basic requirement for an effective photocatalyst, both to enhance the adsorption of reactants and to offer a large number of reactive sites. The low surface area has seriously decreased the activity of existing $BiVO_4$-based compounds and hindered their widespread use as photocatalysts. It has also been demonstrated that an ordered mesoporous structure is highly desirable for effective photocatalysis. This is because such structures, due to their larger surface area and multiple scattering, enable more light to be harvested and also possess

* Corresponding author. E-mail: jimyu@cuhk.edu.hk; fax: +852 2603-5057; tel.: +852 2609-6268.

(1) Hoffmann, M. R.; Martin, S. T.; Choi, W.; Bahnemann, D. W. *Chem. Rev.* **1995**, *95*, 69.
(2) Wang, X. C.; Yu, J. C.; Chen, Y. L.; Wu, L.; Fu, X. Z. *Environ. Sci. Technol.* **2006**, *40*, 2369.
(3) Li, G. S.; Yu, J. C.; Zhu, J.; Cao, Y. *Microporous Mesoporous Mater.* **2007**, *106*, 278.
(4) Li, H. X.; Li, G. S.; Zhu, J.; Wan, Y. *J. Mol. Catal. A: Chem.* **2005**, *226*, 93.
(5) Zhou, L.; Wang, W. Z.; Liu, S. W.; Zhang, L. S.; Xu, H. L.; Zhu, W. *J. Mol. Catal. A: Chem.* **2006**, *252*, 120.
(6) Smith, H. M. *High Performance Pigments*; Wiley-VCH: Weinheim, Germany, 2002.
(7) Kudo, A.; Omori, K.; Kato, H. *J. Am. Chem. Soc.* **1999**, *121*, 11459.
(8) Kohtani, S.; Koshiko, M.; Kudo, A.; Tokumura, K.; Ishigaki, Y.; Toriba, A.; Hayakawa, K.; Nakagaki, R. *Appl. Catal., B* **2003**, *46*, 573.
(9) Tokunaga, S.; Kato, H.; Kudo, A. *Chem. Mater.* **2001**, *13*, 4624.
(10) Lim, A. R.; Choh, S. H.; Jang, M. S. *J. Phys.: Condens. Matter* **1995**, *7*, 7309.
(11) Liu, J. B.; Wang, H.; Wang, S.; Yan, H. *Mater. Sci. Eng., A* **2003**, *104*, 36.
(12) Sayama, K.; Nomura, A.; Zou, Z.; Abe, R.; Abe, Y.; Arakawa, H. *Chem. Commun. (Cambridge, U.K.)* **2003**, 2908.
(13) Zintl, E.; Varino, L. *DRP Patent* **1925**, *422*, 947.

10.1021/cm800236z CCC: $40.75
Published on Web 05/29/2008

continuous pore channels that facilitate the transfer of reactant molecules.[14] The most effective $BiVO_4$ compound from the point-of-view of effective photocatalysis must have both an ordered mesoporous structure and a large surface area. Researchers have been trying to generate such a compound for some time.

Recently, a nanocasting route using ordered mesoporous silica as a hard template was reported for the fabrication of nonsiliceous mesoporous materials.[15] Unlike conventional surfactant templates, the hard templates could effectively maintain the local strain caused by the crystallization of precursors. Such a high stability allows precise inverse replication of templates.[16] The nanocasting strategy, therefore, provides new opportunities for preparing otherwise unobtainable nanosiliceous ordered mesoporous materials.

In this study, ordered mesoporous monoclinic scheelite $BiVO_4$ was fabricated by nanocasting, using 3-D bicontinuous cubic ($Ia\bar{3}d$) mesoporous silica KIT-6 as the replica parent template. The photocatalytic degradation of aqueous methylene blue and oxidation of NO gas in air were then used as a probe reaction to evaluate the photoactivity of the proposed samples. The results of this evaluation demonstrated that the ordered mesoporous $BiVO_4$ sample, because of its large surface area, ordered structure, and small crystal size, had better photocatalytic properties than conventional $BiVO_4$. The most attractive feature of this mesoporous $BiVO_4$ semiconductor was its excellent visible light response ability, with a band gap energy of 2.20 eV.

Experimental Procedures

Preparation of Samples. As-made mesoporous silica KIT-6 was prepared according to procedures reported elsewhere.[17] For a typical synthesis of mesoporous $BiVO_4$, 0.243−0.970 g of $Bi(NO_3)_3 \cdot 5H_2O$ (Aldrich) was dissolved, under ultrasonication in a ultrasonic cleaner, in 10 mL of ethanol containing 0.5 mL of concentrated nitrate acid (69 wt %) to form a transparent colorless solution. A total of 0.083−0.334 g of NH_4VO_3 (Aldrich) was introduced to the solution under ultrasonication for 30 min to form a bright yellow solution. To the solution was added 0.15 g of KIT-6 dry sample. Upon immersion of the silica hard template, the precursor solution diffused into the mesoporous channels of the template by capillary action. The mixture was then heated to dryness over a 12 h period at 80 °C. The dried hybrid sample was then calcined at 200 °C for 12 h. Finally, the mesoporous $BiVO_4$ product with a high yield was obtained by solution etching of the silica framework with a 2 M NaOH aqueous solution. The final product was separated by centrifugation and washed with distilled water and ethanol. In addition to KIT-6 silica, other types of mesoporous silica including SBA-15 (*P6mm* space group) and SBA-16 ($Im\bar{3}m$ space group) also were used as templates to fabricate mesoporous $BiVO_4$. For comparison, conventional $BiVO_4$ synthesized through a hydrothermal process also was prepared.

Characterization. X-ray diffraction (XRD) measurements were carried out in a parallel mode ($\omega = 0.5°$, 2θ varied from 0.5 to 5° and 10 to 60°) using a Bruker D8 Avance X-ray diffractometer (Cu Kα radiation, $\lambda = 1.5406$ Å). The crystal size was estimated from the Scherrer equation,[18] $D = K\lambda/[(\beta_s^2 - \beta_e^2)^{1/2} \cos\theta]$, where D is the crystal size, λ is the wavelength of the X-ray radiation (0.1541 nm) and K usually is taken as 0.89, β_s and β_e are the peak widths at half-maximum height of the sample and the equipment broadening, respectively, and $2\theta = 30.6°$. The N_2-sorption isotherms were recorded at 77 K in a Micromeritics ASAP 2010 instrument. All samples were degassed at 150 °C and 10^{-6} Torr for 24 h prior to measurements. The Brunauer−Emmett−Teller (BET) approach was used to determine the surface area. Standard transmission electron microscopy (TEM) images were recorded using a CM-120 microscope (Philips, 120 kV). The electron microscopy samples were recorded after being prepared by grinding and dispersing the powder in acetone with ultrasonication for 20 s. Carbon-coated copper grids were used as sample holders. Raman spectra were detected by a RenishawRM3000 Micro-Raman system. The diffuse reflectance spectra of the samples over a range of 200−800 nm were recorded by a Varian Cary 100 Scan UV−vis system equipped with a Labsphere diffuse reflectance accessory. X-ray photoelectron spectroscopy (XPS) measurement was performed with a PHI Quantum 2000 XPS system with a monochromatic Al Kα source and a charge neutralizer. All binding energies were referenced to the C_{1s} peak at 284.8 eV of the surface adventitious carbon.

Measurement of Photocatalytic Activity. The photocatalytic degradation of aqueous methylene blue was carried out in an aqueous solution at ambient temperature. Briefly, in a 100 mL beaker, 0.08 g of mesoporous monolith scheelite $BiVO_4$ was suspended in 80 mL of aqueous solution containing 10 ppm methylene blue. The aqueous suspension was stirred for 1 h to reach an adsorption/desorption equilibrium. The photocatalytic degradation of methylene blue was initiated by irradiating the reaction mixture with a commercial 300 W tungsten halogen spotlight surrounded by a filter that restricted the illumination to the 400−660 nm range.[19] Oxygen under atmospheric pressure was bubbled through the reaction continuously. Photodegradation was monitored by measuring the absorbance of the solution at 664 nm.

Photocatalytic activity experiments of the oxidation of NO gas in air were performed at ambient temperature in a continuous flow reactor. The volume of the rectangular reactor, made of stainless steel and covered with Saint-Glass, was 27.3 L (13 cm × 70 cm × 30 cm). Two sample dishes containing the photocatalyst powders were placed on a single path in the reactor. A 300 W commercial tungsten halogen lamp (General Electric) was used as the simulated solar light source. A piece of Pyrex glass was used to cut off the UV light below 400 nm. The lamp was vertically placed outside the reactor above the two sample dishes. Four mini-fans were fixed around the lamp to avoid the temperature rise of the flow system. The photocatalyst samples were prepared by coating an aqueous suspension of our sample onto two dishes with a diameter of 12.0 cm. The weight of the photocatalysts used for each experiment was kept at 0.2 g. The dishes were pretreated at 70 °C until complete removal of water in the suspension and then cooled to room temperature. NO gas was selected as the target pollutant for the photocatalytic degradation at ambient temperature. NO gas was acquired from a compressed gas cylinder at a concentration of 48

(14) Yu, J. C.; Wang, X. C.; Fu, X. Z. *Chem. Mater.* **2004**, *16*, 1523.
(15) (a) Ryoo, R.; Joo, S. H.; Jun, S. J. *J. Phys. Chem. B* **1999**, *103*, 7743. (b) Jun, S.; Joo, S. H.; Ryoo, R.; Kruk, M.; Jaroniec, M.; Liu, Z.; Ohsuna, T.; Terasaki, O. *J. Am. Chem. Soc.* **2000**, *122*, 10712. (c) Shi, Y. F.; Wan, Y.; Liu, R. L.; Tu, B.; Zhao, D. Y. *J. Am. Chem. Soc.* **2007**, *129*, 9522.
(16) (a) Kang, M.; Yi, S. H.; Lee, H. I.; Yie, J. E.; Kim, J. M. *Chem. Commun. (Cambridge, U.K.)* **2002**, 1944. (b) Lu, A.; Schmidt, W.; Taguchi, A.; Spliethoff, B.; Tesche, B.; Schuth, F. *Angew. Chem., Int. Ed.* **2002**, *41*, 3489. (c) Dong, A.; Ren, N.; Tang, Y.; Wang, Y.; Zhang, Y.; Hua, W.; Gao, Z. *J. Am. Chem. Soc.* **2003**, *125*, 4976.
(17) Kleitz, F.; Choi, S. H.; Ryoo, R. *Chem. Commun. (Cambridge, U.K.)* **2003**, 2136.
(18) Weller, M. T. *Inorganic Materials Chemistry*; Oxford University Press: New York, 1994.
(19) Ho, W. K.; Yu, J. C.; Lin, J.; Yu, J. G.; Li, P. S. *Langmuir* **2004**, *20*, 5865.

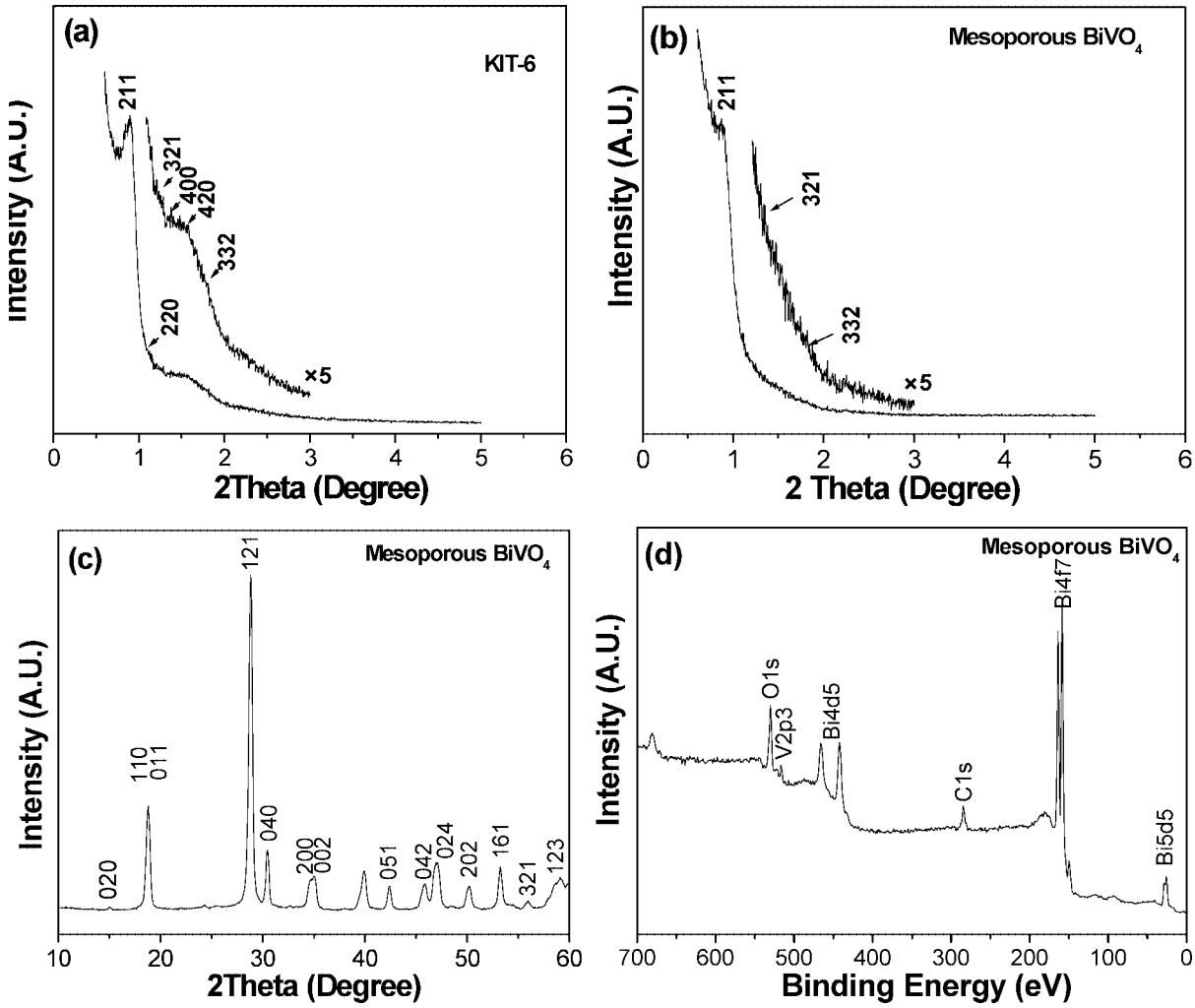

Figure 1. Small-angle XRD patterns of (a) mesoporous cubic KIT-6 silica (space group $Ia\bar{3}d$) and (b) as-prepared mesoporous $BiVO_4$ (silica-free), (c) wide-angle XRD pattern of as-prepared mesoporous $BiVO_4$ (silica-free), and (d) XPS result of as-prepared mesoporous $BiVO_4$.

ppm NO (N_2 balance, BOC gas) with a traceable NIST standard. The initial concentration of NO was diluted to ~400 ppb by the air stream supplied by a zero air generator (Thermo Environmental Inc. Model 111). The desired humidity level of the NO flow was controlled at 70% (2100 ppmv) by passing the zero air streams through a humidification chamber. The gas streams were premixed completely by a gas blender, and the flow rate was controlled at 4 L min^{-1} by a mass flow controller. After the adsorption/desorption equilibrium among water vapor, gases, and photocatalysts was achieved, the lamp was turned on. The concentration of NO was continuously measured by a chemiluminescence NO analyzer (Thermo Environmental Instruments Inc. Model 42c), which monitors NO, NO_2, and NO_x (NO_x represents NO + NO_2) with a sampling rate of 0.7 L/min. The removal rate (%) of NO was defined according to the following equation:

$$\text{NO removal rate (\%)} = ([\text{NO}]_{\text{inlet}} - [\text{NO}]_{\text{outlet}})/[\text{NO}]_{\text{inlet}} \times 100\% \quad (1)$$

where $[NO]_{inlet}$ represents the concentration of NO in the feeding stream and $[NO]_{outlet}$ is the concentration of NO in the outlet stream. The reaction of NO with air was negligible when performing a controllable experiment with or without light in the absence of a photocatalyst.

Results and Discussion

The XRD pattern in Figure 1a shows a highly ordered cubic bicontinuous ($Ia\bar{3}d$) mesostructure in which $a_0 = 22.7$ nm (this calculation being based on the equation of $a_0 = d\{hkl\}(h_2 + k_2 + l_2)^{0.5}$ for KIT-6 prepared by hydrothermal treatment). Upon impregnation of $BiVO_4$ and after the removal of silica by NaOH solution, the final product exhibited a similar, if not so well-resolved, XRD pattern (Figure 1b). This confirms that the $BiVO_4$ replicas have an ordered cubic bicontinuous ($Ia\bar{3}d$) mesostructure. This kind of open mesoporous architecture, with a 3-D connected pore system, is a desirable feature of catalyst design, due to its ability to improve the molecular transport of reactants and products.[20] The cell parameter of the replicas was 21.5 nm, indicating a size shrinkage of ~5%. This suggested that the structural shrinkage for $BiVO_4$ nanocasted from the mesoporous silica scaffold was likely to be very small, regardless of the mother mesostructure. The wide-angle XRD pattern (Figure 1c) demonstrated that the replicas were composed of nanocrystalline monoclinic scheelite $BiVO_4$, as shown in the standard JCPDS No. 14-0688. Furthermore, no tetragonal zircon nor tetragonal scheelite structures were found. Meanwhile, elemental analysis by XPS confirmed the complete removal of silica by the silica-etching process (Figure 1d). The peak of $Si2p_{3/2}$ could not be found in the XPS spectrum of the mesoporous $BiVO_4$. Such a well-defined and pure

(20) Rolison, D. R. *Science (Washington, DC, U.S.)* **2003**, *299*, 1698.

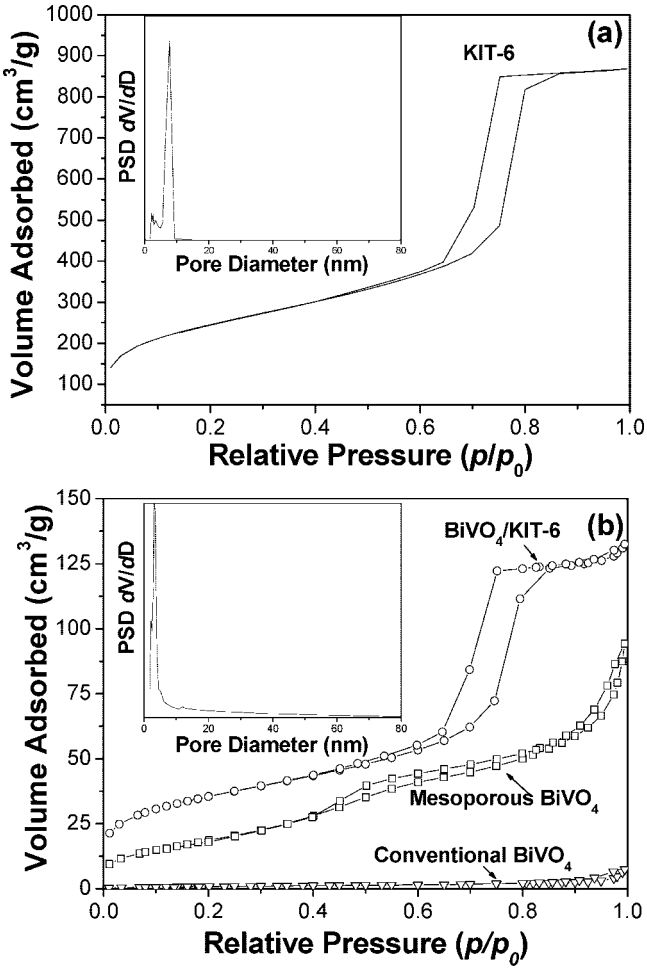

Figure 2. (a) N_2-sorption isotherm and corresponding pore size distribution curves (inset) for replicate template KIT-6, (b) N_2-sorption isotherms for as-prepared mesostructured $BiVO_4$/KIT-6 composite (-○-), mesoporous $BiVO_4$ (-□-), and conventional $BiVO_4$ prepared by hydrothermal process (-▽-) and corresponding pore size distribution curve (inset) for mesoporous $BiVO_4$.

monoclinic scheelite structure is precisely what is required for the effective photocatalytic application of $BiVO_4$.[9] The crystal size of the mesoporous crystalline $BiVO_4$ was estimated to be about 8.0 nm, based on the Scherrer formula,[18] and was much smaller than that of conventional $BiVO_4$ (>100 nm).

Figure 2a,b shows the nitrogen adsorption/desorption isotherms of KIT-6, mesostructured $BiVO_4$/KIT-6 composite, silica-free mesoporous $BiVO_4$, and conventional $BiVO_4$. The isotherms for KIT-6 and mesostructured $BiVO_4$/KIT-6 were of type IV classification. Both had typical hysteresis loops of mesoporous materials. The replicate parent KIT-6 had a surface area of 883 $m^2\ g^{-1}$, a pore volume of 1.33 $cm^3\ g^{-1}$, and a pore size of 7.8 nm (see Table 1), while the mesostructured $BiVO_4$/KIT-6 composite had a much smaller surface area and a pore volume of 127 $m^2\ g^{-1}$ and 0.20 $cm^3\ g^{-1}$, respectively. The pore size, however, decreased only slightly to 7.3 nm. This was because vacancies reappeared in the pores previously filled with the precursor solution after the crystallization of $BiVO_4$. The silica-free mesoporous $BiVO_4$ sample had a surface area of 59 $m^2\ g^{-1}$ and a pore volume of 0.12 $cm^3\ g^{-1}$, much larger than their conventional

Table 1. Physicochemical Properties of As-Prepared Samples

sample	S_{BET} (m^2/g)[a]	pore volume (cm^3/g)[b]	pore size (nm)[c]	a_0 (nm)[d]
KIT-6	883	1.33	7.8	22.7
$BiVO_4$/KIT-6	127	0.2	7.3	
mesoporous $BiVO_4$	59	0.12	3.5	21.5
conventional $BiVO_4$	2			
P25 (Degussa)	51	0.10	8.4	

[a] BET surface area calculated from the linear part of the BET plot ($p/p_0 = 0.1-0.2$). [b] Total pore volumes were estimated from the adsorbed amount at a relative pressure of $p/p_0 = 0.99$. [c] PDS were derived from desorption branches of isotherms using the Barrett−Joyner−Halenda (BJH) method. [d] $a_0 = d\{hkl\}(h_2 + k_2 + l_2)^{0.5}$, in which $d = n\lambda/2 \sin \theta$.

Table 2. Physicochemical Properties of Different Types of Silica and Related Nanocasted Samples

sample	hard template	amount of nanocasted $BiVO_4$(10^{-3} mol)	BET[a] (m^2/g)	pore volume[b] (cm^3/g)	pore size[c] (nm)
	KIT-6	0	883	1.33	7.8
	SBA-15	0	781	1.02	5.2
	SBA-16	0	900	0.58	3.5
$BiVO_4$-1	KIT-6	0.5	42	0.09	3.5
$BiVO_4$-2	KIT-6	1.0	59	0.12	3.5
$BiVO_4$-3	KIT-6	2.0	13	0.03	3.3
$BiVO_4$-4	SBA-15	1.0	19	0.05	3.5
$BiVO_4$-5	SBA-16	1.0	5	0.01	

[a] BET surface area calculated from the linear part of the BET plot ($p/p_0 = 0.1-0.2$). [b] Total pore volumes were estimated from the adsorbed amount at a relative pressure of $p/p_0 = 0.99$. [c] PDS were derived from desorption branches of isotherms using the BJH method.

$BiVO_4$ equivalents (Table 1). Its isotherm was obviously different from that of KIT-6 and $BiVO_4$/KIT-6. The pore size distribution (inset of Figure 2b) was centered at 3.5 nm, reflecting the minimum wall thickness of KIT-6.[17] The wall thickness of the as-prepared materials was calculated by using the relation $b = [1 - V_p\rho/(1 + V_p\rho)]a_0/3.0919$, where ρ is the density (chosen at 1.0 for KIT-6 and mesoporous $BiVO_4$) and V_p is the pore volume.[21] The calculated wall thicknesses of KIT-6 and mesoporous $BiVO_4$ were 3.2 and 6.2 nm, respectively. The calculated pore wall of KIT-6 was very similar to the pore size of $BiVO_4$ of 3.5 nm. Some large mesopores with an average pore size of 13 nm also were found to be present, and their presence was doubtless attributable to the wall junctions in KIT-6.[22]

Mesoporous silica templates with three different pore space groups—KIT-6 ($Ia\bar{3}d$), SBA-15 ($P6mm$), and SBA-16 ($Im\bar{3}m$)—were tested. SBA-15 has been widely used in the fabrication of mesoporous materials.[23] Although the surface area, pore volume, and pore size of SBA-15 were similar to those of KIT-6, the mesoporous $BiVO_4$ nanocasted by SBA-15 exhibited a relatively small surface area and pore volume (see Table 2). Our results indicated that the two-dimensional SBA-15 structure was not as effective as KIT-6 for nanocasting mesoporous $BiVO_4$. In the case of SBA-16, the nanocasted $BiVO_4$ had a very small pore volume and pore size. The narrow pore size of only 3.5 nm, just half of that of KIT-6, seriously limited the growth of $BiVO_4$ in the pore

(21) (a) Ravikovitch, P. I.; Neimark, A. V. *Langmuir* **2000**, *16*, 2419. (b) Dibandjo, P.; Chassagneux, F.; Bois, L.; Sigala, C.; Miele, P. *Microporous Mesoporous Mater.* **2006**, *92*, 286.
(22) Jiao, K.; Zhang, B.; Yue, B.; Ren, Y.; Liu, S. X.; Yan, S. R.; Dickinson, C.; Zhou, W. Z.; He, H. Y. *Chem. Commun. (Cambridge, U.K.)* **2005**, 5618.
(23) Lu, A. H.; Schüth, F. *Adv. Mater.* **2006**, *18*, 1793.

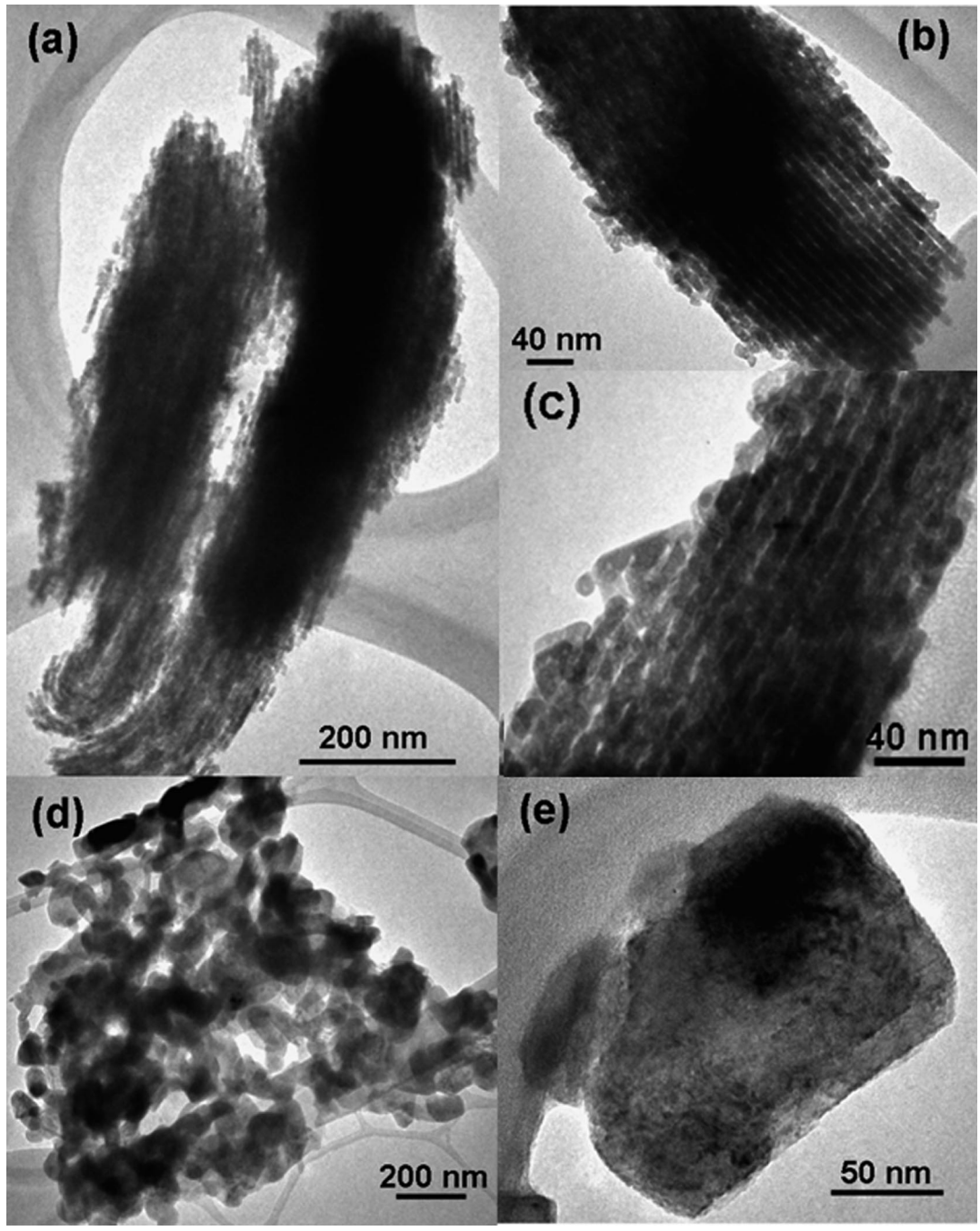

Figure 3. (a−c) TEM images of as-prepared mesoporous $BiVO_4$. (d and e) TEM images of conventional $BiVO_4$ prepared by a hydrothermal process.

channels. As shown in Table 2, the best combination was KIT-6 and 1.0 mol of nanocasted $BiVO_4$.

The TEM images in Figure 3a−c show clearly the periodic ordered channels of $BiVO_4$. The ordered mesopores and the evenly spaced parallel channels confirmed a well-developed long-range order consistent with the XRD results. The crystal size of $BiVO_4$ was estimated to be ∼7.5 nm. This result was in good agreement with the evaluation obtained using a Scherrer equation based on the XRD patterns. Furthermore, the crystals formed the pore wall of mesoporous $BiVO_4$. The pore wall thickness estimated from the TEM images was about 7.5 nm, slightly higher than the 6.2 nm calculated from the BET result. The difference between the two values for the pore wall thickness may be due to an error inherent in the calculation method based on the BET result. Conventional $BiVO_4$ had a much larger crystal size than mesoporous $BiVO_4$, ranging from 100 to 200 nm (Figure 3d,e). This was due to uncontrolled crystal growth in the absence of ordered mesoporous channels. We therefore speculate that the formation of ordered mesoporous $BiVO_4$ is related to the evaporation process in which the precursor is introduced into the silica pores (this kind of nanocasting approach has been widely used for the fabrication of mesoporous metal oxides, metal sulfate, and carbon).[15c,23] The evaporation process thus formed a precursor/KIT-6 nanocomposite. During the heat treatment process, the confined pore space of the parent template slowed down the formation rate of $BiVO_4$. Upon the proper nanocasting amount, the ordered mesostructure

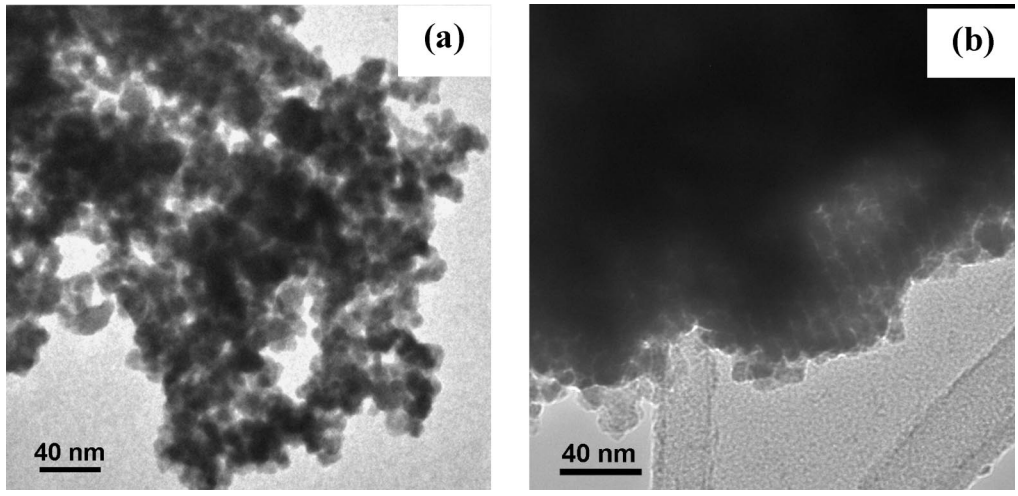

Figure 4. TEM images of as-prepared mesoporous $BiVO_4$ precursor using KIT-6 as a template nanocasting with 0.5 mol of precursor (a) and with 2.0 mol of precursor (b).

Scheme 1. Proposed Process for Fabrication of Mesoporous $BiVO_4$

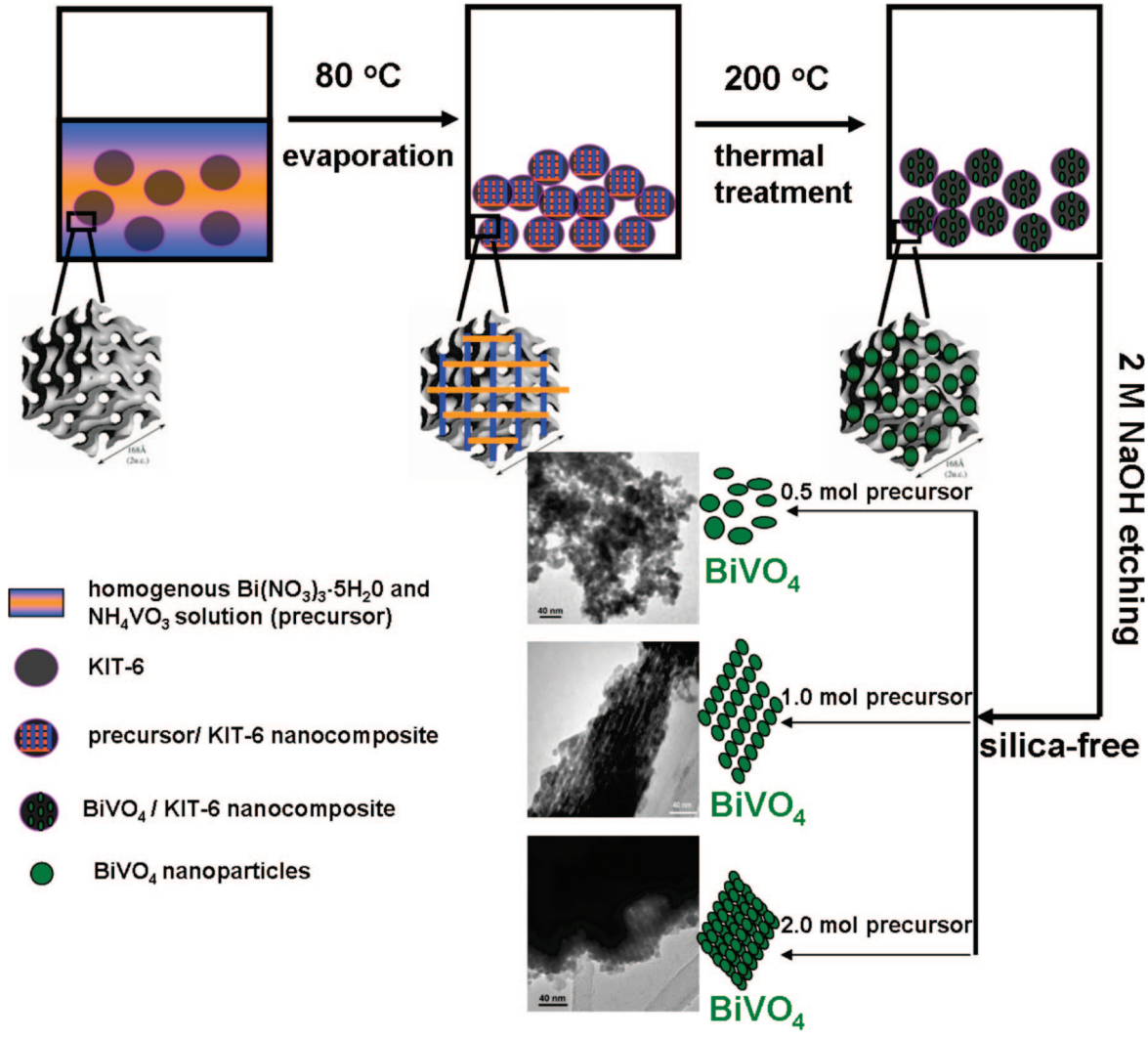

was retained after the removal of the template (Scheme 1). Meanwhile, the morphologies of as-prepared mesoporous $BiVO_4$ nanocasted with varying amounts of $BiVO_4$ precursors using KIT-6 as a template also were investigated by TEM. Figure 4a shows the TEM image of the mesoporous $BiVO_4$ nanocasted with 0.5 mol of the precursor. Obviously, a long-range order mesoporous structure could not be found, although the mesoporous structures could still be seen clearly. This is probably attributable to the collapse of the $BiVO_4$ pore wall located in the channels of silica during the silica-etching process as a result of the incomplete filling of the $BiVO_4$ precursor in the pore channels when an insufficient

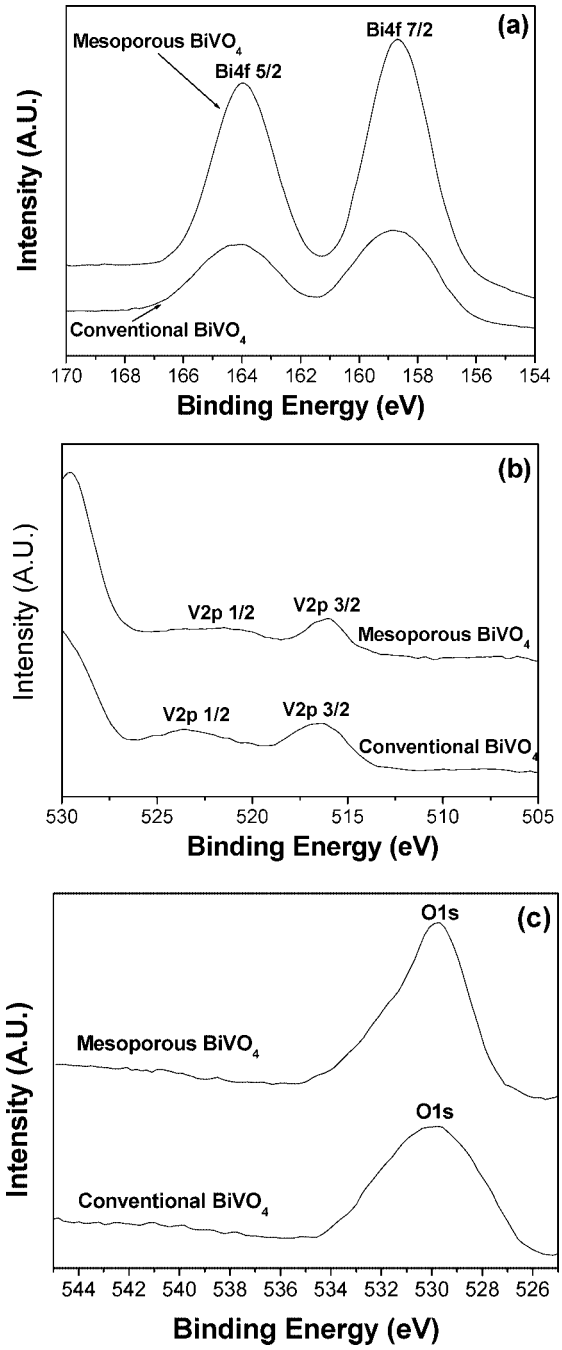

Figure 5. XPS analysis of Bi4f (a), V2p (b), and O1s (c) for as-prepared mesoporous $BiVO_4$ and conventional $BiVO_4$ prepared by the hydrothermal process.

precursor (0.5 mol) was used. This result also demonstrates that the mesopores were formed between intra-agglomerated primary particles.[24] By contrast, when an excess $BiVO_4$ precursor of 2.0 mol was used, superfluous $BiVO_4$ aggregated outside the channels of mesoporous silica (Figure 4b).

The XPS spectra of the as-prepared mesoporous and conventional samples (Figure 5) show the characteristic spin−orbit split of the Bi4f5/2 and Bi4f7/2 signals (Figure 5a), V2p1/2 and V2p3/2 signals (Figure 5b), and the O1s peak (Figure 5c). The binding energies of the different elements are attributable to the typical monoclinic scheelite

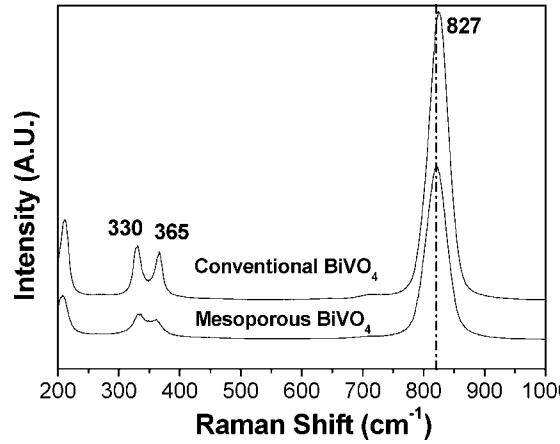

Figure 6. Raman spectra of (a) as-prepared mesoporous $BiVO_4$ and (b) conventional $BiVO_4$ prepared by the hydrothermal process.

$BiVO_4$. In this respect, the observed O1s peak at 529.8 eV can be attributed to the lattice oxygen in crystalline $BiVO_4$.[25] Raman scattering spectra of the crystalline $BiVO_4$ samples are shown in Figure 6. Raman bands at 330, 365, and 827 cm^{-1} were observed in the spectrum of the conventional $BiVO_4$ sample prepared by the hydrothermal method. These Raman bands represented the typical vibration bands of monoclinic scheelite $BiVO_4$ and could be assigned to the asymmetric and symmetric deformation modes of VO_4^{3-} and the symmetric stretching mode of the V−O bond, respectively.[26] However, the Raman bands of mesoporous $BiVO_4$ were slightly different from those of the conventional sample. The deformation modes of VO_4^{3-} overlapped with each other, and the relative intensities of the 330 and 365 cm^{-1} peaks were greatly decreased. Meanwhile, the stretching mode of the V−O bond shifted from 827 to 820 cm^{-1}. The peak position red-shifts might be attributable to the quantum size confinement effect of the mesoporous $BiVO_4$ material for its ultrafine nanoscale crystal grains.[27] Such a phenomenon was earlier predicted by Richter et al., on purely theoretical grounds.[28] The natural Lorentzian phonon band characteristics of infinite solids (bulk) evolve into an asymmetric Raman band when the physical size of the solid-state system decreases. Many examples of asymmetric Raman bands in confined particles[29] and wires[30] also have been reported.

The electronic structure of the semiconductor plays a crucial role in its photocatalytic activity.[31] For monoclinic scheelite $BiVO_4$, the valence band (VB) is formed by a hybridization of the Bi6s and O2p orbitals, while the

(24) Ho, W. K.; Yu, J. C.; Lee, S. C. *Chem. Commun. (Cambridge, U.K.)* **2006**, *10*, 1115.
(25) Zhang, L.; Chen, D. R.; Jiao, X. L. *J. Phys. Chem. B* **2006**, *110*, 2668.
(26) (a) Galembeck, A.; Alves, O. L. *Thin Solid Films* **2000**, *365*, 90. (b) Sleight, A. W.; Chen, H. Y.; Ferretti, A. *Mater. Res. Bull.* **1979**, *14*, 1571.
(27) (a) Ma, Z. X.; Liao, X. B.; Kong, G. L.; Chu, J. H. *Sci. China, Ser. A* **2000**, *43*, 414. (b) Adu, K. W.; Gutierrez, H. R.; Eklund, P. C. *Vib. Spectrosc.* **2006**, *42*, 165.
(28) Richter, H.; Wang, Z. P.; Ley, Y. *Solid State Commun.* **1981**, *39*, 625.
(29) (a) Adu, K. W.; Gutierrez, H. R.; Kim, U. J.; Eklund, P. C. *Nano Lett.* **2005**, *5*, 409. (b) Noborisaka, J.; Motohisa, J.; Hara, S.; Fukui, T. *Appl. Phys. Lett.* **2005**, *87*, 93109.
(30) Gupta, R.; Axing, Q.; Adu, C. K.; Kim, U. J.; Eklund, P. C. *Nano Lett.* **2003**, *3*, 627.
(31) (a) Fu, H. B.; Pan, C. S.; Yao, W. Q.; Zhu, Y. F. *J. Phys. Chem. B* **2005**, *109*, 22432. (b) Wang, D. F.; Tang, J. W.; Zou, Z. G.; Ye, J. H. *Chem. Mater.* **2005**, *17*, 5177.

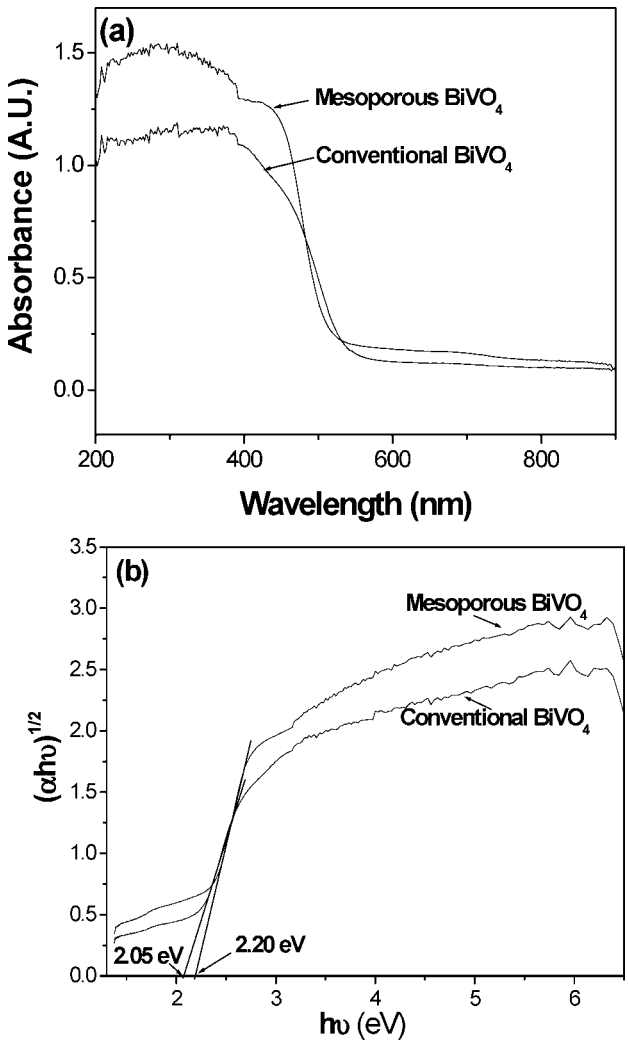

Figure 7. UV−vis absorption spectra of (a) and determination of indirect interband transition energies (b) for as-prepared mesoporous $BiVO_4$ and conventional $BiVO_4$ prepared by the hydrothermal process.

conduction band is composed of V3d orbitals. Upon photoexcitation, charge transfer occurs from the Bi6s and O2p hybrid orbitals to the V3d orbitals.[32] The largely dispersed VB, owing to the hybridization of the Bi6s and O2p levels, can facilitate the mobility of photoexcited holes, thereby improving the rate of photocatalytic oxidation of organic pollutants.[33]

UV−vis diffuse reflectance spectroscopy (DRS) was used to characterize the electronic states of the as-prepared samples. Figure 7a shows the UV−vis absorption spectra of mesoporous $BiVO_4$ prepared by the nanocasting route and also the hydrothermally prepared conventional $BiVO_4$. Figure 7b shows the optical absorption edges (in eV) of the two samples. Both samples exhibited absorption bands in the visible light region, the characteristic absorption pattern of monoclinic scheelite $BiVO_4$.[7] The steep shape of the spectrum indicated that the visible light adsorption was due to the band gap transition.[34] Unlike conventional $BiVO_4$, the absorption edge of the mesoporous $BiVO_4$ blue-shifted (i.e., shifted to shorter wavelengths). The band gap energies were, respectively, estimated from the $(a\hbar\nu)^{1/2}$ versus photon energy plots to be 2.20 eV for mesoporous $BiVO_4$ and 2.05 eV for conventional $BiVO_4$. The optical band energy of mesoporous $BiVO_4$ (2.20 eV) exhibited an obvious blue-shift with respect to that of conventional $BiVO_4$ (2.05 eV). This may be ascribed to the decrease of the crystal size for mesoporous $BiVO_4$ (quantum size effect (QSE)).[35] QSEs are known to occur for semiconductor particles (Q-particles) on the order of 1−10 nm in size. The anomalies arise when the size of the semiconductor particles becomes comparable to the de Broglie wavelength of the charge carriers in the semiconductor. The range of size for particles experiencing QSE is therefore dependent on the effective mass for the Q-particle semiconductor. The electron and hole produced in Q-particles are confined in a potential well of small geometrical dimensions and do not experience electronic delocalization present in a bulk semiconductor possessing a conduction band and a valence band. Instead, the confinement produces a quantization of discrete electronic states and increases the effective band gap of the semiconductor. Such effects can change the color of the material (due to the altered optical absorption maxima) and its photocatalytic properties.[35] It is therefore reasonable to assume that the increase of band gap for mesoporous $BiVO_4$ is due to its quantum size effect because the particle size of mesoporous $BiVO_4$ (~8 nm) has been located in the scale of quantum size as compared to that of bulk $BiVO_4$ (>100 nm). The band gap of $BiVO_4$ may undergo a slight change upon adsorption of reactant molecules during a photocatalytic reaction. Oshikiri and Boero reported that the adsorbed water molecules could slightly decrease the band gap of a $BiVO_4$ film.[36] Nevertheless, such small shifts of band gap energy do not affect the use of mesoporous $BiVO_4$ as a visible light-driven photocatalyst. Interestingly, mesoporous $BiVO_4$ exhibited a much stronger absorption in the visible light region (especially 400−500 nm) than conventional $BiVO_4$. This was because its ordered mesoporous structure, enlarged surface area, and multiple scattering enabled it to harvest light much more efficiently.[14] This enhanced light-trapping effect was the result of the reflection or transmission of light scattered by the mesopores implanted in the $BiVO_4$ body. A similar effect was verified in porous silicon wafers.[37] It is therefore a reasonable assumption that the quantum efficiency of bulk $BiVO_4$ can perhaps also be increased through improving the porosity and surface area of $BiVO_4$ to enhance its light-trapping effect. The results of this study therefore indicate that the enhanced ability of this type of mesoporous $BiVO_4$ to absorb visible light makes it a promising photocatalyst for solar-driven applications.

The photocatalytic activities of ordered mesoporous and conventional $BiVO_4$ samples were measured in both liquid-phase and gas-phase reactions. The decomposition of methylene blue in an aqueous solution was chosen as the

(32) Oshikiri, M.; Boero, M.; Ye, J. H.; Zou, Z. G.; Kido, G. *J. Chem. Phys.* **2002**, *117*, 7313.
(33) Tang, J. W.; Zou, Z. G.; Ye, J. H. *Angew. Chem., Int. Ed.* **2004**, *43*, 4463.
(34) Zhang, C.; Zhu, Y. F. *Chem. Mater.* **2005**, *17*, 3537.
(35) Linsebigler, A. L.; Lu, G. Q.; Yates, J. T. *J. Chem. Rev.* **1995**, *95*, 735.
(36) Oshikiri, M.; Boero, M. *J. Phys. Chem. B* **2006**, *110*, 9188.
(37) Abouelsaood, A. A. *J. Appl. Phys.* **2002**, *91*, 2357.

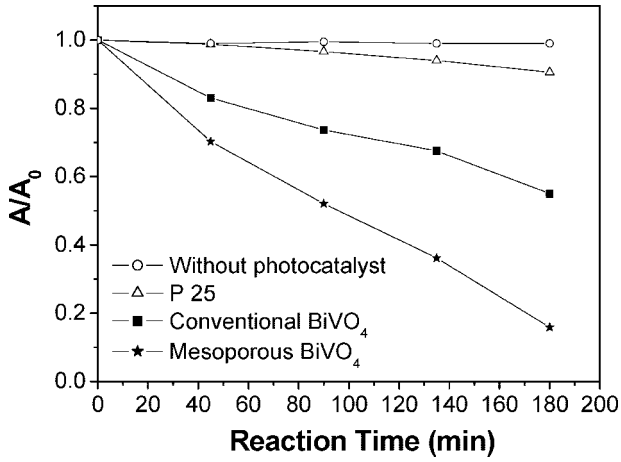

Figure 8. Comparison of the photoactivities of P25 (Degussa) (-△-), conventional $BiVO_4$ (-■-), mesoporous $BiVO_4$ (-∗-), and without photocatalyst (-○-). *A* is the absorbance of methylene blue ($\lambda_{max} = 664$ nm), and A_0 is the initial absorbance.

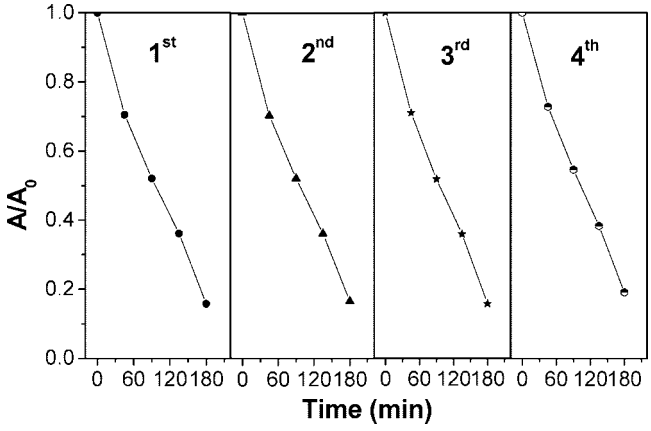

Figure 9. Cyclability of mesoporous $BiVO_4$.

photoreaction probe. Figure 8 shows that the degradation rates of both conventional and mesoporous $BiVO_4$ were much higher than that of commercial P25 (Degussa) under the irradiation of visible light (400 nm $< \lambda <$ 660 nm). On average, mesoporous $BiVO_4$ was twice as active as conventional $BiVO_4$.

To investigate the recyclability of the mesoporous $BiVO_4$ photocatalyst, sample powders after photocatalytic reactions were collected by centrifugation and dried for the subsequent photoreaction cycle. As shown in Figure 9, mesoporous $BiVO_4$ showed an excellent stability and maintained a broadly similar level of photocatalytic activity after four reaction cycles. The ability of the photocatalysts to oxidize NO gas in air also was studied. Figure 10 shows the rates of NO removal after a single pass through the reactor. The rate for mesoporous $BiVO_4$ was ∼3 times faster than that for conventional $BiVO_4$. However, the NO removal rate decreased slowly after about 50 min, probably due to the accumulation of HNO_3 on the catalyst surface that deactivated the as-prepared photocatalysts. Similar phenomena have been reported before.[38] Meanwhile, the cyclability of mesoporous $BiVO_4$ for NO removal in a single pass flow of

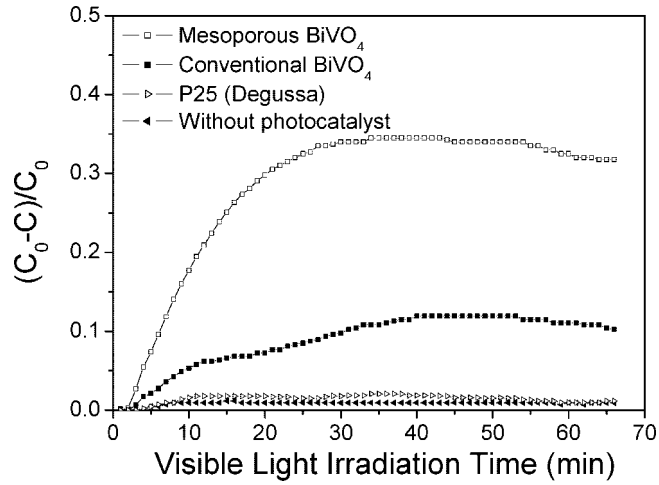

Figure 10. NO removal rate of as-prepared photocatalysts in a single pass flow of air.

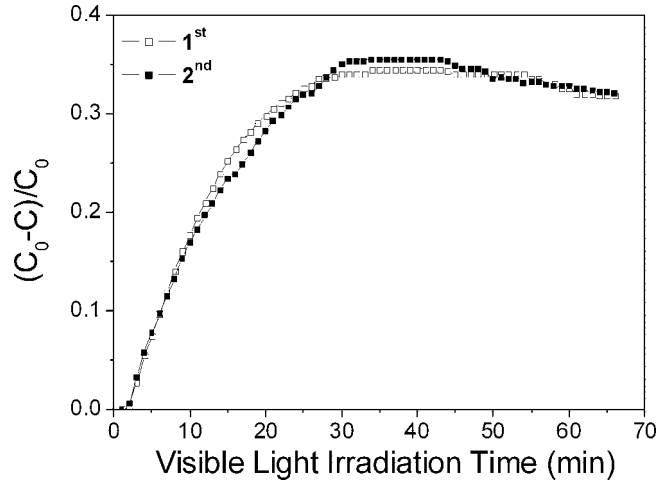

Figure 11. Cyclability of mesoporous $BiVO_4$ for NO removal in a single pass flow of air.

air also is shown in Figure 11. The NO removal rate for mesoporous $BiVO_4$ was well-maintained.

The enhanced activity of mesoporous $BiVO_4$ is due to its physicochemical properties such as crystal size, BET surface area, and pore structure. Generally, the small crystal size allows for more efficient transfer of electron−holes generated inside the crystal to the surface. A large surface area not only supplies more active sites for the degradation reaction of organic compounds but also effectively promotes the separation efficiency of the electron−hole pairs, resulting in a higher quantum efficiency of the photocatalytic reaction.[39] Meanwhile, light also is harvested more effectively due to the large surface area and multiple scattering.[14] The high catalytic activity also is related to the open ordered mesoporous architecture with a 3-D connected pore system. Chemical reactions are most effective when the transport paths through which molecules move into or out of the nanostructured materials are included as an integral part of the architectural design.[40] Such 3-D interconnected mesochannels in mesoporous $BiVO_4$ provide efficient transport paths

(38) (a) Ao, C. H.; Lee, S. C. *Appl. Catal., B* **2003**, *44*, 191. (b) Ibusuki, I.; Yakeuchi, K. *J. Mol. Catal. A: Chem.* **1994**, *88*, 93.

(39) (a) Tang, J. W.; Zou, Z. G.; Ye, J. H. *Chem. Mater.* **2004**, *16*, 1644. (b) Yu, J. G.; Xiong, J. F.; Cheng, B.; Liu, S. W. *Appl. Catal., B* **2005**, *60*, 211.

for reactants and products in photocatalytic reactions.[41] The mesostructure stays intact after gaseous-phase photocatalytic measurements. While a more vigorous agitation during solution-phase degradation of methylene blue does cause some large particles to break up, the mesopores are nevertheless preserved in these fragments. The VO_4^{3-} tetrahedron is distorted by the lone-pair electron of Bi^{3+} in the local structure of $BiVO_4$. This distortion significantly enhances the hybridization of the Bi6s and O2p orbitals,[42] and a strong hybridization effect can in turn effectively accelerate the migration of photogenerated holes.[32,33] Therefore, the recombination rate of the photogenerated electron−hole pairs can be decreased. More holes can be utilized in the degradation reaction.

Conclusion

In this study, a new mesoporous monolith scheelite $BiVO_4$ was fabricated by a nanocasting method. The ordered mesoporous structure was confirmed by XRD, TEM, and N_2 adsorption measurements. The sample possessed a large surface area, an ordered structure, and a small crystal size, resulting in excellent visible light photocatalytic activity.

Acknowledgment. This research was supported by a Strategic Investments Scheme administrated by The Chinese University of Hong Kong. Prof. S. C. Lee's group is thanked (Department of Civil and Structural Engineering of The Hong Kong Polytechnic University) for their assistance in the oxidation of NO gas measurements.

CM800236Z

(40) Bell, A. T. *Science (Washington, DC, U.S.)* **2003**, *299*, 1688.
(41) Yu, J. C.; Li, G. S.; Wang, X. C.; Hu, X. L.; Leung, C. W.; Zhang, Z. D. *Chem. Commun. (Cambridge, U.K.)* **2006**, 2717.
(42) Yu, J. Q.; Kudo, A. *Adv. Funct. Mater.* **2006**, *16*, 2163.